E/*Z* ISOMERIZATION OF 3-HYDRAZONOCAMPHOR PROMOTED BY COORDINATION TO PALLADIUM OR PLATINUM

M. Fernanda N. N. CARVALHO[1,*], Ana S. D. FERREIRA[2], João L. Ferreira da SILVA[3] and Luís F. VEIROS[4]

Centro de Química Estrutural, Complexo I, Instituto Superior Técnico, Universidade Técnica de Lisboa, Av. Rovisco Pais, 1049-001 Lisboa, Portugal; e-mail: [1] fcarvalho@ist.utl.pt, [2] sofia.ferreira@gmail.com, [3] joao.luis@ist.utl.pt, [4] veiros@ist.utl.pt

Received February 12, 2007
Accepted March 31, 2007

Dedicated to Dr Karel Mach on the occasion of his 70th birthday in recognition of his outstanding contribution to the area of coordination chemistry.

3-Hydrazonocamphor, 3-(RR^1NN)$C_{10}H_{14}O$ (R = Me, R^1 = H), undergoes intramolecular hydrogen bridging by coordination to platinum or palladium. This effect is evidenced by considerable decrease in the ν(C=O) frequency (compared to the free ligand) in the IR spectra of the complexes [MCl_2L_2] (M = Pd, Pt; L = 3-(RR^1NN)$C_{10}H_{14}O$) as well as by the magnetic non-equivalence of the two ligands, as revealed by ^{13}C NMR. DFT calculations indicate that coordination of 3-(Me(H)NN)$C_{10}H_{14}O$ promotes *E*/*Z* isomerization of the hydrazono group of the ligand, inducing formation of intramolecular hydrogen bonding and corresponding stabilization of the complex. Characterization of the complexes [MCl_2L_2] (M = Pt; L: R, R^1 = Me (**1**), R = Me, R^1 = H (**2**) and M = Pd; L: R = Me, R^1 = H (**3**)) was performed by analytical and spectroscopic techniques. Redox properties of the 3-hydazonocamphors and their complexes were studied by cyclic voltammetry. The structure of *trans*-[$PtCl_2${3-(Me_2NN)$C_{10}H_{14}O$}$_2$] was determined by single-crystal X-ray diffraction analysis. The complex has square-planar geometry and crystallizes in the tetragonal $P4_3$ space group.

Keywords: Platinum complexes; Palladium; Camphorimine; Hydrazones; Hydrogen bonding; DFT calculations; Cyclic voltammetry; IR spectroscopy.

The complex *trans*-[$PdCl_2${3-(Me_2NN)$C_{10}H_{14}O$}$_2$] is an efficient and selective catalyst for cyclotrimerization of alkynes[1,2] and formation of heterocycles[3] from alkynols, while related *trans*-[$PdCl_2${3-(PhN)$C_{10}H_{14}O$}$_2$] displays no catalytic activity. Previous studies have shown[2] that the ability of camphor-derived complexes *trans*-[$PdCl_2L_2$] (Chart 1) to promote the coordinative activation of alkynes strongly depends on the characteristics of the hydrazono group.

Collect. Czech. Chem. Commun. 2007, Vol. 72, Nos. 5–6, pp. 649–665

doi:10.1135/cccc20070649

The goal of this study is to get a deeper insight into the coordinative ability of the 3-hydrazonocamphor ligands L1 and L2, and to correlate it with the properties of their Pt and Pd complexes. The syntheses and detailed characterization of the complexes are presented.

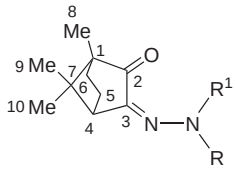

CHART 1
3-Hydrazonocamphor (L: R, R^1 = Me (L1); R = Me, R^1 = H (L2))

RESULTS AND DISCUSSION

Syntheses and Characterization of Pt and Pd Complexes

MCl_2 (M = Pt, Pd) reacts slowly with an appropriate 3-hydrazonocamphor ligand L (Chart 1) in chlorinated solvents (dichloromethane or 1,2-dichloroethane), affording complexes *trans*-$[MCl_2L_2]$ (M = Pt: L = L1 (**1**), L = L2 (**2**); M = Pd: L = L2 (**3**)). The kinetics of the reactions follows inverse trends for palladium and platinum, i.e. L2 reacts faster than L1 with $PtCl_2$, while the inverse trend is followed with $PdCl_2$ (see Experimental).

Published experimental procedures[4] to prepare L2 have been improved and spectral characterization by IR and NMR spectroscopies is reported in Experimental.

The structure of *trans*-$[PtCl_2\{3\text{-}(Me_2NN)C_{10}H_{14}O\}_2]$ (L = L1; **1**) was obtained by single-crystal X-ray diffraction analysis. Complex **1** crystallizes in the tetragonal $P4_3$ space group and has a square-planar geometry. The L1 ligands and the two chloride atoms occupy mutually trans positions (Fig. 1) at distances from the metal in the expected range (Pt–N 2.004, 2.024 Å; Pt–Cl 2.3006, 2.3054 Å)[5].

The 3-hydrazonocamphor ligands coordinate platinum through the double-bonded nitrogen atom, while the oxygen atoms of the keto groups of the camphor skeleton approach the apical sites at the metal at distances in the range of the sum of the platinum and oxygen van der Waals radii (Pt–O2 3.087 Å, Pt–O1 3.033 Å). This feature gives to the complex some pseudooctahedral character, as corroborated by the angle (86.2°) established by planes (N1, N3, Cl1, Cl2) and (N1, N3, O1, O2), which is close to

TABLE I
X-ray structural data of complex **1**

Bond length, Å		Bond angle, °	
Pt–N(3)	2.004(4)	N(3)–Pt–N(1)	178.87(19)
Pt–N(1)	2.024(4)	N(3)–Pt–Cl(1)	89.39(14)
Pt–Cl(1)	2.3006(18)	N(1)–Pt–Cl(1)	90.77(13)
Pt–Cl(2)	2.3054(19)	N(3)–Pt–Cl(2)	91.27(13)
N(3)–C(13)	1.285(7)	N(1)–Pt–Cl(2)	88.63(13)
N(1)–C(1)	1.278(6)	C(13)–N(3)–Pt	126.2(4)
N(1)–N(4)	1.461(7)	Cl(1)–Pt–Cl(2)	177.25(11)
N(2)–N(1)	1.431(6)	C(13)–N(3)–N(4)	111.8(4)
N(4)–C(23)	1.428(10)	N(4)–N(3)–Pt	122.0(3)
N(4)–C(24)	1.449(9)	N(1)–C(1)–C(6)	129.6(5)
N(2)–C(11)	1.465(8)	N(2)–N(1)–Pt	122.8(3)
N(2)–C(12)	1.467(8)		
		Non-bonding distance, Å	
Pt–O(2)	3.087	Pt–H(11)	2.809
Pt–O(1)	3.033	O(2)–H(11)	2.546

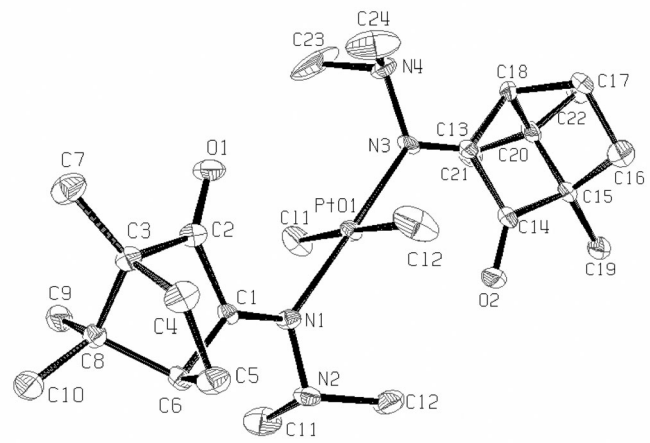

FIG. 1
ORTEP drawing showing the labeling scheme for *trans*-[$PtCl_2${3-(Me_2NN)$C_{10}H_{14}O$}$_2$] (**1**)

90°. This effect was also observed in related 3-hydrazonocamphor palladium complexes[2,6]. Comparing the basal plane in complexes *trans*-[MCl_2L_2] (M = Pt, Pd; L = L1) we conclude that the distortion is smaller in Pt complex **1** (Pt atom 0.017 Å out of the best least-squares plane) than in the Pd complexes[2]. Selected bond lengths and angles for complex **1** are listed in Table I.

In the absence of structural data, the characterization of complexes **2** and **3** relies mostly on IR and NMR (^{1}H, ^{13}C and DEPT, HSQC, HMBC) spectral data (Table II).

The IR spectra of the complexes show strong to medium absorption bands in the region 1752–1577 cm^{-1}, which are attributed to ν(C=O) and ν(C=N) modes of the 3-hydrazonocamphor ligand. Complex **1** exhibits positive shifts in ν(C=O) and ν(C=N) compared to the free ligands (Table II) such as all hydrazonocamphor complexes reported till now. A positive shift in ν(C=N) is expected upon coordination of the hydrazonocamphor to the metal center due to electron release from the C=N moiety, thereby enforcing the sp^2 character of the coordinating nitrogen atom (see DFT calculations below). In the absence of other effects, a positive shift in ν(C=O) is also expected due to the M···O=C– interaction and concomitant electron release towards the metal center.

The character of the metal determines the magnitude of the shifts in the IR spectra, i.e., platinum induces larger ν(C=N) shifts than palladium (Pt: 57 cm^{-1}; Pd: 43 cm^{-1} (ref.[6])). The same trend applies for the ν(C=O) shifts (Pt: 45 cm^{-1}; Pd: 43 cm^{-1} (ref.[6])); although, the difference is less pronounced in this case as the keto group is not coordinated.

TABLE II
Relevant spectral data for complexes *trans*-[MCl_2L_2] **1**–**3** and ligands L1 and L2

trans-[MCl_2L_2]		R, R^1	IR (ν, cm^{-1})			^{13}C NMR (δ, ppm)[a]	
			ν(NH)	ν(C=O)	ν(C=N)	CO	CN
M = Pt	**1**	Me, Me	–	1752	1624	201.4	176.0
	2	Me, H	3255	1678	1577	202.1 201.8	151.5 151.1
M = Pd	**3**	Me, H	3267	1689	1578	201.3 201.0	149.7 150.2
L[b]	L1	Me, Me	–	1707	1567	205.0	143.1
	L2	Me, H	3232	1714	1579	204.2	145.4

[a] In $CDCl_3$, δ values versus TMS. [b] See ref.[6].

For complexes **2** and **3**, negative shifts in ν(C=N) and ν(C=O) were observed compared to the free ligands. Moreover, the shift in ν(C=N) is very small (ca. 1–2 cm^{-1}; Table I) while the shift in ν(C=O) is of the order (36 cm^{-1}) observed for complex **1** but in the opposite direction. These unexpected results drew our attention to the relation between the characteristics of the 3-hydrazonocamphor ligand and the properties of the complexes.

On the absence of structure details for complexes **2** or **3**, we inspected in more detail the X-ray data of complex **1**. We realized that one hydrogen atom of a methyl group at the singly bound N of L1 (Chart 1) is close to the oxygen of the keto group and to the platinum atoms at the distance Pt–O(2)–H(N–CH_3) within the sum of the van der Waals radii of the atoms (tolerance 0.1 Å; Table I). In complexes with ligand L2 (where a methyl group was replaced by hydrogen), such interaction could in principle be favored. Hydrogen bonding, either intra- or intermolecular, involving the keto group, could account for the negative shift observed in the IR spectra of complexes **2** and **3**. To probe intermolecular interactions, the IR spectra of **2** were obtained in CH_2Cl_2 or C_6H_6. Negative ν(C=O) shifts (1694 and 1696 cm^{-1}, respectively) were measured, thereby discarding intermolecular interactions as the major contributor to the IR shifts observed in the solid state.

DFT Calculations

DFT calculations[7] were performed in order to rationalize the unexpected negative ν(C=N) and ν(C=O) shifts observed for complexes **2** and **3**. The performance of the theoretical method (see Computational Details) was tested through optimization of the geometry of complex **1** and comparison with the corresponding X-ray structure (see above). The agreement between the optimized and experimental geometries is remarkably good, with maximum and mean absolute deviations for all bonding distances between non-hydrogen atoms reaching 0.06 and 0.02 Å, respectively.

Based on the good performance of the computational method in the description of the studied system from the structural point of view, the ν(C=N) and ν(C=O) wavenumbers were calculated for complex **1**. These values were used to calibrate the frequencies calculated for all the other species (see Computational Details).

The optimized structures obtained for the two studied 3-hydrazonocamphor ligands L1 and L2, the corresponding C=N and C=O distances, Wiberg indices[8] (WI) and computed ν(C=N) and ν(C=O) wavenumbers are displayed in Fig. 2.

The corresponding pairs of C=N and C=O bonds in L1 and L2 are equivalent, the distances and Wiberg indices being very close, within 0.002 Å and 0.03, respectively. The Wiberg indices, well above 1.5 for both bonds, indicate strong double bond characters. The calculated ν(C=N) and ν(C=O) frequencies, compare well (within 7–24 cm^{-1}) with the experimental results in Table II. It should be noted that the compound used to calibrate the calculated frequencies was complex **1** that includes Pt and Cl. These elements are described by a basis set that uses effective core potentials (ECP) to describe the core electrons. These elements are absent in the non-coordinate ligand that contains only C, N and O (described by an all-electron basis set). Thus, a better agreement between calculated and experimental frequencies is expected for complexes $[PtCl_2L_2]$ as systems for which the frequency scale factor has been obtained. This is particularly true given the known sensibility of calculated frequencies to the basis set[9].

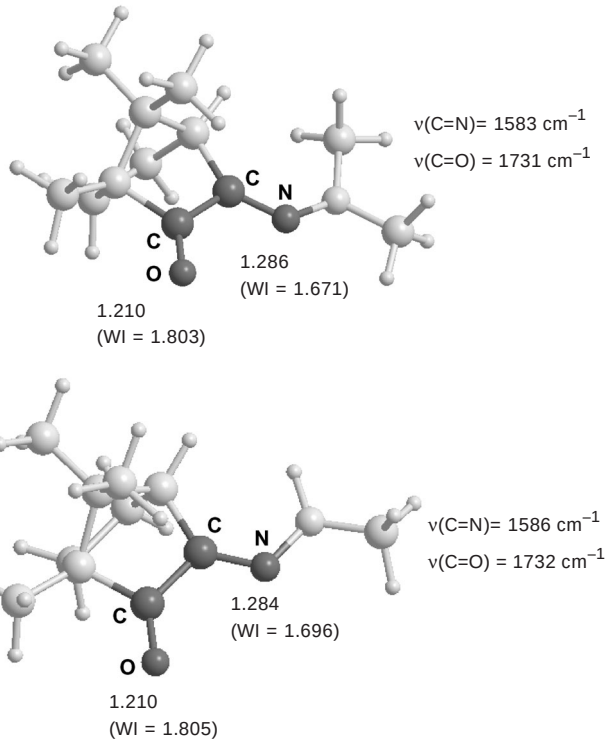

FIG. 2

Optimized geometries (PBE1PBE) for 3-hydrazonocamphor ligands L1 (R, R^1 = Me) and L2 (R = Me, R^1 = H). The C=N and C=O bonds are drawn darker and the corresponding distances (in Å), Wiberg indices (WI) and ν(C=N)/ν(C=O) frequencies are presented

A marked positive shift is observed between the frequencies calculated for ligand L1 (Fig. 2) and those calculated for complex **1** (ν(C=N) 1624 cm^{-1} and ν(C=O) 1753 cm^{-1}), in agreement with the experimental observations (see above). This is a direct result of the strengthening of the C=N and C=O bonds upon coordination. The C=N bond length becomes diminished from 1.286 Å in L1 to 1.278/1.280 Å in complex **1**, getting stronger, as shown by the Wiberg indices: 1.67 for L1 and 1.71/1.72 for **1**. The same applies for the C=O bond: $d_{C=O}$ = 1.210 Å and WI = 1.803 for L1, and $d_{C=O}$ = 1.204 Å and WI = 1.84 for **1**.

The optimized structures obtained for Pd complex **2** (i.e., **2a**, **2b** and **2c**) are given in Fig. 3. The three isomers considered differ in the orientation of the Me(H)N substituent in L2. For **2a**, both L2 ligands show *E*-configuration of the Me(H)N substituent, bringing it to the opposite side of the carbonyl group. In **2c**, the two L2 ligands have *Z*-configuration that brings the Me(H)N substituent and the C=O group to close proximity. Isomer **2b** has one L2 ligand in the *Z*-configuration and the other in the *E*-configuration.

The structural characteristics of the three isomers of complex **2** (Fig. 3) are equivalent and display square-planar geometry with the 3-hydrazonocamphor ligands L2 coordinated to the metal through the double-bonded nitrogen, as verified for **1** by X-ray crystallography (Fig. 1).

The Pt–N bond lengths obtained for complexes **2a**–**2c** (1.99–2.02 Å) are similar to those optimized for complex **1** (2.01 Å). The same applies for the Pt–Cl bond lengths: 2.36 and 2.37 Å in **1**, and 2.34–2.36 Å in **2a**–**2c**.

The most relevant difference between the three isomers (**2a**, **2b** and **2c**) of complex **2** is the geometry of the ligands L2. In fact, in the cases where L2 adopts a cis arrangement (one ligand in **2b** and two in **2c**), an intramolecular hydrogen bridge (N–H···O) forms with short O···H (1.84–1.86 Å) contacts. The C=N and C=O bonds of the ligands involved in the hydrogen bonding reflect these interactions, becoming significantly longer and weaker than those in non-coordinated L2 (see Figs 2 and 3 for relevant bond lengths and Wiberg indices). At the same time, when the ligand adopts a trans arrangement (two in **2a** and one in **2b**), strengthening of the C=N and C=O bonds results from coordination, similarly to what is observed with complex **1** (see above). In complex **1**, the ligand L1, the Me_2N group is the substituent on the double-bonded N and, thus, the possibility of formation of the hydrogen bridge following a change of the ligand arrangement is precluded.

The formation of the hydrogen bridges in complex **2** results in an overall stabilization of the molecule. The calculated relative energy shows that there is an average stabilization of ca. 8 kcal mol^{-1} per each hydrogen

bridge formed (Fig. 3). Consequently, the most stable isomer is that with the two hydrogen bridges (**2c**) while the least stable is that with lacking hydrogen bridge (**2a**), i.e., the one with the two ligands L2 keeping the trans arrangement.

Comparing the calculated frequency values for the isomer **2c** (Fig. 3) with the experimental data for complex **2** (Table II), an almost perfect match is

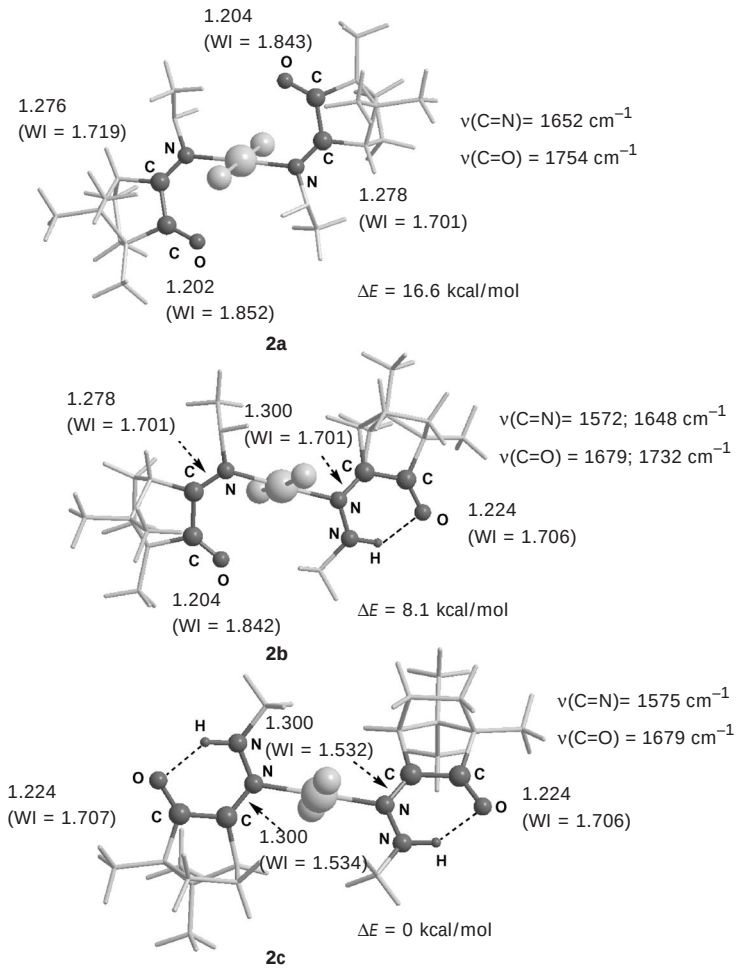

FIG. 3

Optimized geometries (PBE1PBE) and relative energies (in kcal mol^{-1}) obtained for three isomers of complex **2**, depending on the arrangement of the 3-hydrazonocamphor ligands L2: *E*,*E* (**2a**), *Z*,*E* (**2b**) and *Z*,*Z* (**2c**). The C=O and C=N bonds are drawn darker and the corresponding distances (in Å), Wiberg indices (WI) and calculated ν(C=N)/ν(C=O) frequencies are presented

observed for ν(C=N) and ν(C=O) (differences of 1–2 cm^{-1}), indicating that the geometry of complex **2** corresponds to isomer **2c**, which is also the most stable one. There is no experimental evidence for isomer **2b** higher in energy, since in that case two sets of ν(C=N) and ν(C=O) frequencies should be observed (which is not the case), one corresponding to L2 in the cis arrangement and the other to L2 in the trans arrangement. The calculated differences between ν(C=N) (76 cm^{-1}) and ν(C=O) (53 cm^{-1}) for trans and cis L2 in **2b** should be observable by IR spectroscopy.

The optimized structure of the cis L2 conformer was calculated in order to probe intramolecular bonding in the free ligand. The results show a short O···H contact of 1.96 Å (Fig. 4), in agreement with the intramolecular hydrogen bonding. Moreover, all features previously discussed for coordinated L2 in complexes **2a**–**2c** are maintained in the free ligand.

Comparing the calculated values for the free trans L2 and cis L2 conformers, longer and weaker C=N and C=O bonds exist in the cis L2 conformer, which agrees with the lower IR ν(C=N) and ν(C=O) frequencies by 42 and 66 cm^{-1}, respectively. In ligand L2, such as bound in complexes **2a**–**2c**, the formation of the intramolecular hydrogen bond brings extra stability to the molecule and the cis conformer is indeed more stable by 6.1 kcal mol^{-1} than the trans conformer.

In the syntheses of complexes **2** and **3**, the less stable trans L2 conformer was used, as confirmed by their IR spectra with the ν(C=N) and ν(C=O) values considerably higher (35 and 48 cm^{-1}, respectively; Table II) than those calculated for the cis L2 conformer.

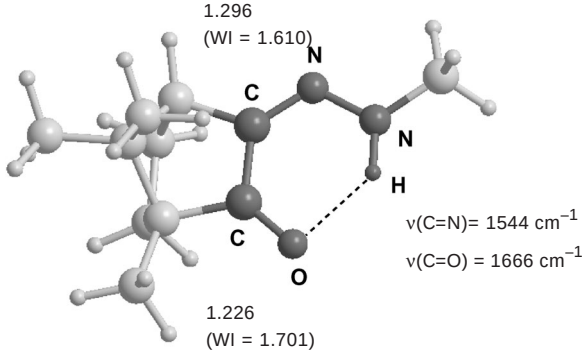

FIG. 4
Optimized geometry (PBE1PBE) for the cis L2 conformer. The C=N and C=O bonds are drawn darker and the corresponding distances (in Å), Wiberg indices (WI) and ν(C=N)/ν(C=O) frequencies are presented

The DFT calculations indicate that coordination to the metal center promotes the isomerization of the 3-hydrazonocamphor ligand L2 from the trans to the cis form. This effect results in a considerable stabilization of the molecule due to the formation of a six-membered ring as consequence of hydrogen bonding, which is responsible for the negative ν(C=O) shift observed in the IR spectra of complexes **2** and **3**.

As a consequence of the hydrogen bonding, the L2 ligands in *trans*-$[MCl_2(L2)_2]$ **2** or **3** become non-equivalent. Thus, by ^{13}C NMR, two sets of signals attributed to distinct ketone carbon atoms (201.3, 201.0 (**2**); 202.1, 201.8 (**3**)) and to N–carbon atoms (149.7, 150.2 (**2**); 151.5, 151.1 (**3**)) are observed. In addition, the methyl groups (C-9 or C-10) as well as the C-4 carbon atom of the camphor skeleton also become non-equivalent in the two L2 ligands (Fig. 5). This behavior was not observed for so far known non-hydrogen-bridged hydrazonocamphor complexes that exhibit just a single set of signals for each type of carbon atom.

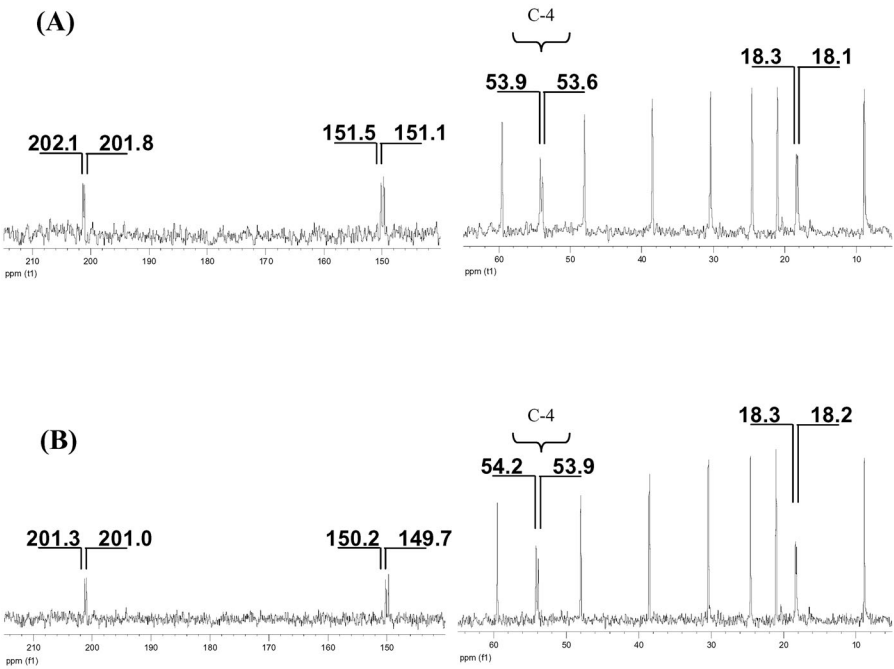

FIG. 5
Details of ^{13}C NMR spectra of: A $[PtCl_2(L2)_2]$ (**2**) and B $[PdCl_2(L2)_2]$ (**3**)

Cyclic Voltammetry

The electrochemical properties of complexes **1**, **2** and **3** and their precursor ligands (L1, L2) were studied by cyclic voltammetry in acetonitrile/Bu_4NPF_6 using a Pt wire as working electrode (see Experimental).

Within the available potential range, all complexes and ligands display at least one cathodic and one anodic (except complex **1**) irreversible waves (Table III). Ligand L2 and its complexes **2** and **3** display a second cathodic process at lower potentials. The higher-potential cathodic processes in Pt complexes (**1** and **2**) are at the same electrode potentials (E_p^{red} = –1.57 V vs F_c/F_c^+) which is considerably lower than that measured for Pd complex **3** (E_p^{red} = –0.99 V) or for the related complex *trans*-[$PdCl_2(L1)_2$] (E_p^{red} = –1.2 V)[6].

In the complexes, the higher cathodic potentials are expected for metal-based reductions, i.e. more negative values for Pt than Pd complexes. Controlled-potential electrolysis (CPE) of complex **3** at –1.0 V led to deposition of palladium metal upon transfer of two electrons per molecule, hence corroborating the $M^{II} \rightarrow M^0$ reduction process.

The lower-potential cathodic process in complexes **2** or **3** (Pt: –1.94 V, Pd: –2.04 V) occurs at values close to that of the free ligand L2 (–1.96 V), hence suggesting a ligand-based process. Both the LUMO and LUMO+1 of complex **2**, obtained by DFT, show a high participation of the ligand (Fig. 6), but only the LUMO+1 contains a significant metal contribution.

TABLE III
Electrochemical data[a] for complexes *trans*-[MCl_2L_2] (M = Pt: L = L1 (**1**), L = L2 (**2**); M = Pd: L = L2 (**3**)) and ligands L1 and L2

Complex	E_p^{red}, V	E_p^{ox}, V	Ligand	E_p^{red}, V	E_p^{ox}, V
1	–1.57	–	L1	–2.42	1.15
2	–1.57 –1.94	1.88	L2	–1.96	1.30
3	–0.99 –2.04[b]	1.84			

[a] Values (±10 mV) measured in acetonitrile/0.1 M Bu_4NBF_4 against ferrocene as internal reference: F_c/F_c^+ = 0.38 V vs SCE [10]. [b] Displays partly reversible character, $E_{1/2}^{red}$ = –1.99 V.

The experimental data obtained by CPE of complex **3** point to inversion between the LUMO and LUMO+1, since the first cathodic process involves reduction of the metal. The electrolyte solution apparently overcomes the energy difference (0.4 eV) between these orbitals, accounting for the observed experimental behavior.

The anodic processes in complexes **2** and **3** occur at considerably different potentials compared to ligand L2. Moreover, no anodic wave was detected for complex **1.** The metal NPA charges calculated for **1** (0.64) and **2c** (0.61) indicate a more positive metal center in complex **1**, in agreement with a higher oxidation potential, most likely out of the available range. The HOMO obtained by DFT for both **1** and **2c** is delocalized on the metal and the two chloride ligands, corresponding to a π^* molecular orbital resulting from the interaction between metal d and chloride p orbitals, and representing π-donation from Cl to Pt.

Further studies are necessary to ascertain if there is an effect of trans/cis isomerization of ligand L2 on the redox or catalytic properties of complexes **2** and **3**, such as documented for their spectroscopic properties (IR, NMR) of the complexes. The stabilization introduced by hydrogen bonding in complexes *trans*-$[MCl_2(L2)_2]$ (M = Pt, Pd) may affect the ability to activate cyclization of alkynes or heterocycle formation from alkynols.

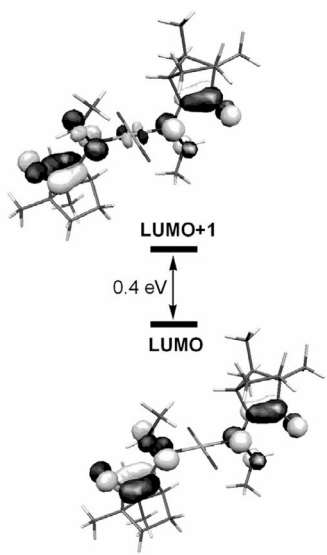

FIG. 6
LUMO+1 and LUMO of complex **2c**

EXPERIMENTAL

All experiments were carried out under nitrogen, using standard vacuum and Schlenck techniques.

The solvents were purchased from Fischer Scientific or Panreac, purified by conventional techniques[11] and distilled before use. $PdCl_2$ and $PtCl_2$ (98%) were purchased from Riedel–de Haën and Aldrich, respectively.

NMR spectra (δ, ppm; *J*, Hz) were obtained in $CDCl_3$ using a Varian 300 spectrometer. TMS (δ 0) was used as internal reference. IR spectra were obtained with a JASCO FTIR 430 spectrometer.

Cyclic voltammetry and controlled potential electrolyses were carried out with a VoltaLab PST050 Radiometer Analytical set-up, using a Pt wire and Pt gauze working electrodes, respectively. The electrolyte was 0.1 M solution of Bu_4NBF_4 in acetonitrile. Electrode potentials were determined versus ferrocene as internal standard, which can be converted to the SCE scale using $E_{1/2}$ (F_c/F_c^+) = 0.38 V [10].

Computational Details

All calculations were performed using the Gaussian 03 software package[12] and the PBE1PBE functional without symmetry constraints. The functional uses a hybrid generalized gradient approximation (GGA), including 25% mixture of Hartree–Fock[13] exchange with DFT[7] exchange-correlation, given by the Perdew, Burke and Ernzerhof functional (PBE)[14]. The optimized geometries were obtained with the LanL2DZ basis set[15] augmented with a f-polarization function[16], for Pt, and the same basis set augmented with a d-polarization function[17] for Cl. The remaining elements were described by the standard 4-31G(d,p)[18] basis set. A natural population analysis (NPA)[19] and the resulting Wiberg indices[8] were used to study the electronic structure and bonding of the optimized species. All frequencies reported in the main text have been scaled by a factor of 0.926. This scale factor was obtained from the ratio of the experimental ν(C=N) and ν(C=O) values measured for complex **1** and those calculated for the same species at 1754 (ν(C=N)) and 1893 cm^{-1} (ν(C=O)). Orbital representations were obtained using the program MOLEKEL 4.0 [20].

X-ray Crystallographic Analysis

X-ray crystallographic data were collected from orange crystals, using an area-detector diffractometer (Bruker AXS-KAPPA APEX II) equipped with an Oxford Cryosystem open-flow nitrogen cryostat at 150 K and graphite-monochromated MoKα (λ = 0.71073 Å) radiation. Crystals had good quality and diffracting power, presenting a low R_{int} (0.0438) value that allowed low *R* values ($R_{1(all)}$ = 0.053 and $R_{1(obs)}$ = 0.039). Unit cell dimensions were obtained using Bruker SMART software. All the reflections were refined with Bruker SAINT programs[21]. Absorption corrections were applied using SADABS [22]. The structures were solved by direct methods with SIR97 [23] using full-matrix least-squares refinement against F2 with SHELXL97 [24]. All the programs belong to the WINGX package (version 1.64.05)[25]. All non-hydrogen atoms were refined anisotropically, and the hydrogen atoms were inserted in idealized positions. Drawings were made with ORTEP3 for Windows[26].

Relevant details for the X-ray data analysis are in Table IV.

CCDC 630369 (**1**) contains the supplementary crystallographic data for this paper. These data can be obtained free of charge via www.ccdc.cam.ac.uk/conts/retrieving.html (or from

TABLE IV
Crystal data and structure refinement for *trans*-[$PtCl_2${3-(Me_2NN)$C_{10}H_{14}O$}$_2$] (**1**)

Empirical formula	$C_{24}H_{40}Cl_2N_4O_2Pt$
Formula weight, g mol^{-1}	682.59
Temperature, K	150
Wavelength, Å	0.71073
Crystal system	tetragonal
Space group	$P4_3$
Unit cell dimensions	
a, Å	9.841(5)
b, Å	9.841(5)
c, Å	28.363(5)
Volume, Å^3	2747(2)
Z	4
Calculated density, Mg m^{-3}	1.651
Absorption coefficient, mm^{-1}	5.330
F(000)	1360
Crystal size, mm	0.2 × 0.2 × 0.4
θ range for data collection, °	2.07–30.53
Index ranges	$-8 \le h \le 14$; $-12 \le k \le 13$; $-38 \le l \le 37$
Reflections collected/unique	19437/7806 [R_{int} = 0.0438]
Completeness to θ = 30.53	96.7%
Refinement method	full-matrix least-squares on F^2
Data/restraints/parameters	7806/1/288
GOF on F^2	1.004
Final *R* indices [$I > 2\sigma(I)$]	R_1 = 0.0390, wR_2 = 0.0665
R indices (all data)	R_1 = 0.0528, wR_2 = 0.0696
Absolute structure parameter	0.016(7)
Largest diff. peak and hole, e Å^{-3}	1.246 and –1.529

the Cambridge Crystallographic Data Centre, 12, Union Road, Cambridge, CB2 1EZ, UK; fax: +44 1223 336033; or deposit@ccdc.cam.ac.uk).

Syntheses of Complexes **1**–**3**

trans-[PtCl$_2${3-(Me$_2$NN)C$_{10}$H$_{14}$O}$_2$] (**1**). A suspension of $PtCl_2$ (0.15 g, 0.56 mmol) and 3-(Me_2NN)$C_{10}H_{14}O$ (0.297 g, 1.43 mmol) (L1) was heated under reflux in dichloroethane (70 cm^3) for 5 days. The suspension was filtrated to remove traces of unreacted $PtCl_2$ and the solvent was evaporated to ca. 2 cm^3. Complex **1** precipitates as orange crystals by addition of Et_2O (20 cm^3), followed by overnight cooling (–18 °C). Crystals were filtered off and washed with Et_2O (2 × 2 cm^3). Yield 0.108 g (16%). For $C_{24}H_{40}Cl_2N_4O_2Pt \cdot 0.25(CH_2Cl)_2$ (707.3) calculated: 41.6% C, 5.8% H, 7.9% N; found: 41.7% C, 6.2% H, 7.9% N. IR: see Table II. ^{1}H NMR: 3.40 d, 2 H, *J* = 5.1 (H-4); 3.16 s, 12 H ($N(CH_3)_2$); 2.08–1.45 m, 8 H (H-5,6); 1.08 s, 6 H (CH_3-8); 0.96, 0.97 s, 12 H (CH_3-9,10). ^{13}C NMR: 201.4 (CO); 176.0 (CN); 58.8 (C-1); 54.0 (C-4); 48.3 ($N(CH_3)_2$); 44.1 (C-7); 30.2, 24.3 (C-5,6); 17.9, 21.1 (C-9,10); 9.5 (C-8) (see Chart 1 for labeling). A further crop of the product was obtained on solvent evaporation and addition of Et_2O. Total yield ca. 25%.

trans-[PtCl$_2${3-(Me(H)NN)C$_{10}$H$_{14}$O}$_2$] (**2**). A suspension of $PtCl_2$ (0.145 g, 0.545 mmol) and 3-(Me(H)NN)$C_{10}H_{14}O$ (0.320 g, 1.65 mmol) (L2) was stirred under reflux in 1,2-dichloroethane (60 cm^3) for 3 days. The suspension was filtered to remove traces of $PtCl_2$ and the solvent was evaporated to ca. 5 cm^3. Et_2O was added and compound **2** precipitated by cooling (–18 °C). Upon filtration the yellow title compound was obtained. Yield 0.114 g (32%). For $C_{22}H_{36}Cl_2N_4O_2Pt$ (654.1) calculated: 40.4% C, 5.5% H, 8.6% N; found: 40.5% C, 5.4% H, 8.3% N. IR: see Table II. ^{1}H NMR: 10.1 s br, 2 H (N**H**CH_3); 4.102 d, 1 H, 4.039 d, 1 H, *J* = 3.7 (H-4); 3.676 d, 3 H, *J* = 3.1, 3.640 d, 3 H, *J* = 3.7 (NHC**H**$_3$); 2.22–1.21 m, 8 H (H-5,6); 0.98 s, 6 H (CH_3-8); 1.00, 0.92 s, 12 H (CH_3-9,10). ^{13}C NMR: 202.1, 201.8 (CO); 151.5, 151.1 (CN); 59.3 (C-1); 53.6, 53.9 (C-4); 47.9 (C-7); 37.9 ($NHCH_3$); 24.5, 30.4 (C-5,6); 21.3, 18.3, 18.1 (C-9,10); 8.9 (C-8) (see Chart 1 for labeling).

trans-[PdCl$_2${3-(Me(H)NN)C$_{10}$H$_{14}$O}$_2$] (**3**). A suspension of $PdCl_2$ (0.15 g, 0.86 mmol) and 3-(Me(H)NN)$C_{10}H_{14}O$ (0.502 g, 2.59 mmol) (L2) was stirred in dichloromethane (60 cm^3) for 3 days. The suspension was filtered to remove traces of $PdCl_2$ and the solvent was evaporated to ca. 5 cm^3. Complex **3** was formed as a yellow precipitate by addition of Et_2O (10 cm^3), which was filtrated off and washed with Et_2O. Yield 0.443 g (84%). For $C_{22}H_{36}Cl_2N_4O_2Pd \cdot 0.5CH_2Cl_2$ (607.9) calculated: 44.4% C, 6.1% H, 9.2% N; found: 44.3% C, 6.6% H, 9.1% N. IR: see Table II. ^{1}H NMR: 9.686 d, 1 H, 9.637 d, 1 H, *J* = 3.7 (N**H**CH_3); 4.094 d, 1 H, *J* = 3.1, 4.064 d, 1 H, *J* = 3.7 (H-4); 3.79 t, 6 H, *J* = 4.9 (NHC**H**$_3$); 2.22–1.41 m, 8 H (H-5,6); 1.02, 0.96 s, 12 H (CH_3-9,10); 0.90 s, 6 H (CH_3-8). ^{13}C NMR: 201.3, 201.0 (CO); 149.7, 150.2 (CN); 59.5 (C-1); 54.2, 53.9 (C-4); 48.0 (C-7); 38.5 ($NHCH_3$); 21.0, 18.3, 18.2 (C-9,10); 8.8 (C-8) (see Chart 1 for labeling).

Synthesis of 1,7,7-Trimethyl-3-(methylhydrazono)bicyclo[2.2.1]heptan-2-one Ligand L2

Methylhydrazine (0.12 cm^3, 2.13 mmol) was added to a solution of 1,7,7-trimethylbicyclo-[2.2.1]heptane-2,3-dione (camphorquinone) (0.25 g, 1.5 mmol) in EtOH (1 cm^3). The mixture was stirred at ca. 40 °C for 1 day. The solvent and excess of methylhydrazine were evaporated in vacuo and the oily solid dissolved in hexane (30 cm^3). A white precipitate of L2 was filtered off and dried. Yield 0.19 g (65%). IR: see Table II. ^{1}H NMR: 5.6 s, 1 H

(N**H**CH_3); 3.15 s, 3 H (NHC**H**$_3$); 2.65 d, 1 H, *J* = 4.5 (H-4); 2.13–1.14 m, 4 H (H-5,6); 0.97, 0.94 s, 6 H (CH_3-9,10); 0.83 s, 3 H (CH_3-8). ^{13}C NMR: 204.2 (CO); 145.4 (CN); 57.8 (C-1); 45.9 (C-7); 45.1 (C-4); 37.7 ($NHCH_3$); 31.6, 23.7 (C-5,6); 20.4, 18.1 (C-9,10); 9.1 (C-8) (see Chart 1 for labeling).

This work was partially supported by Fundação para a Ciência e Tecnologia (FCT) and FEDER under POCI 2010 (Project POCI/QUI/58119/2004).

REFERENCES AND NOTES

1. Carvalho M. F. N. N., Almeida F. M. T., Galvão A. M., Pombeiro A. J. L.: *J. Organomet. Chem.* **2003**, *679*, 143.
2. Carvalho M. F. N. N., Duarte M. T., Herrmann R.: *Collect. Czech. Chem. Commun.* **2006**, *71*, 302.
3. Carvalho M. F. N. N., Ferreira A. S. D., Herrmann R.: *J. Organomet. Chem.* **2006**, *691*, 4124.
4. Forster M. O., Thornley T.: *J. Chem. Soc.* **1909**, *95*, 942.
5. Allen F. H.: *Acta Crystallogr., Sect. B: Struct. Sci.* **2002**, *58*, 380.
6. Carvalho M. F. N. N., Costa L. M. G., Pombeiro A. J. L., Schier A., Scherer W., Harbi S. K., Verfürth U., Herrmann R.: *Inorg. Chem.* **1994**, *33*, 6270.
7. Parr R. G., Yang W.: *Density Functional Theory of Atoms and Molecules*. Oxford University Press, New York 1989.
8. a) Wiberg K. B.: *Tetrahedron* **1968**, *24*, 1083; b) Wiberg indices are electronic parameters related to the electron density between atoms. They can be obtained by a natural population analysis. They provide a measure of the bond strength.
9. a) Foresman J. B., Frisch A. E.: *Exploring Chemistry with Electronic Structure Methods*, 2nd ed. Gaussian Inc., Pittsburgh (PA) 1996; b) Tantirungrotechai Y., Phanasant K., Roddecha S., Surawanawong P., Sutthikhum V., Limtrakul J.: *J. Mol. Struct. (TEOCHEM)* **2006**, *760*, 189.
10. Aranzaes J. R., Daniel M.-C., Astruc D.: *Can. J. Chem.* **2006**, *84*, 288.
11. Perrin D. D., Amarego W. L. F., Perrin D. R.: *Purification of Laboratory Chemicals*, 2nd ed. Pergamon Press, Ltd., Oxford 1980.
12. Frisch M. J., Trucks G. W., Schlegel H. B., Scuseria G. E., Robb M. A., Cheeseman J. R., Montgomery J. A., Vreven T., Jr., Kudin K. N., Burant J. C., Millam J. M., Iyengar S. S., Tomasi J., Barone V., Mennucci B., Cossi M., Scalmani G., Rega N., Petersson G. A., Nakatsuji H., Hada M., Ehara M., Toyota K., Fukuda R., Hasegawa J., Ishida M., Nakajima T., Honda Y., Kitao O., Nakai H., Klene M., Li X., Knox J. E., Hratchian H. P., Cross J. B., Adamo C., Jaramillo J., Gomperts R., Stratmann R. E., Yazyev O., Austin A. J., Cammi R., Pomelli C., Ochterski J. W., Ayala P. Y., Morokuma K., Voth G. A., Salvador P., Dannenberg J. J., Zakrzewski V. G., Dapprich S., Daniels A. D., Strain M. C., Farkas O., Malick D. K., Rabuck A. D., Raghavachari K., Foresman J. B., Ortiz J. V., Cui Q., Baboul A. G., Clifford S., Cioslowski J., Stefanov B. B., Liu G., Liashenko A., Piskorz P., Komaromi I., Martin R. L., Fox D. J., Keith T., Al-Laham M. A., Peng C. Y., Nanayakkara A., Challacombe M., Gill P. M. W., Johnson B., Chen W., Wong M. W., Gonzalez C., Pople J. A.: *Gaussian 03*, Revision C.02. Gaussian, Inc., Wallingford (CT) 2004.

13. Hehre W. J., Radom L., Schleyer P. v. R., Pople J. A.: *Ab Initio Molecular Orbital Theory*. John Wiley & Sons, New York 1986.
14. a) Perdew J. P., Burke K., Ernzerhof M.: *Phys. Rev. Lett.* **1997**, *78*, 1396; b) Perdew J. P.: *Phys. Rev. B* **1986**, *33*, 8822.
15. a) Dunning T. H., Jr., Hay P. J. in: *Modern Theoretical Chemistry* (H. F. Schaefer III, Ed.), Vol. 3, p. 1. Plenum, New York 1976; b) Hay P. J., Wadt W. R.: *J. Chem. Phys.* **1985**, *82*, 270; c) Wadt W. R., Hay P. J.: *J. Chem. Phys.* **1985**, *82*, 284; d) Hay P. J., Wadt W. R.: *J. Chem. Phys.* **1985**, *82*, 2299.
16. Ehlers A. W., Böhme M., Dapprich S., Gobbi A., Höllwarth A., Jonas V., Köhler K. F., Stegmann R., Veldkamp A., Frenking G.: *Chem. Phys. Lett.* **1993**, *208*, 111.
17. Höllwarth A., Böhme M., Dapprich S., Ehlers A. W., Gobbi A., Jonas V., Köhler K. F., Stegmann R., Veldkamp A., Frenking G.: *Chem. Phys. Lett.* **1993**, *208*, 237.
18. a) Ditchfield R., Hehre W. J., Pople J. A.: *J. Chem. Phys.* **1971**, *54*, 724; b) Hehre W. J., Ditchfield R., Pople J. A.: *J. Chem. Phys.* **1972**, *56*, 2257; c) Hariharan P. C., Pople J. A.: *Mol. Phys.* **1974**, *27*, 209; d) Gordon M. S.: *Chem. Phys. Lett.* **1980**, *76*, 163.
19. a) Carpenter J. E., Weinhold F.: *J. Mol. Struct. (THEOCHEM)* **1988**, *169*, 41; b) Carpenter J. E.: *Ph.D. Thesis*. University of Wisconsin, Madison (WI) 1987; c) Foster J. P., Weinhold F.: *J. Am. Chem. Soc.* **1980**, *102*, 7211; d) Reed A. E., Weinhold F.: *J. Chem. Phys.* **1983**, *78*, 4066; e) Reed A. E., Weinhold F.: *J. Chem. Phys.* **1983**, *78*, 4066; f) Reed A. E., Weinstock R. B., Weinhold F.: *J. Chem. Phys.* **1985**, *83*, 735; g) Reed A. E., Curtiss L. A., Weinhold F.: *Chem. Rev.* **1988**, *88*, 899; h) Weinhold F., Carpenter J. E.: *The Structure of Small Molecules and Ions*, p. 227. Plenum, New York 1988.
20. Flükiger P., Lüthi H. P., Portmann S., Weber J.: Swiss Center for Scientific Computing, Manno (Switzerland) 2000.
21. *SMART and SAINT: Area Detector Control and Integration Software*. Bruker AXS, Madison (WI) 2004.
22. Sheldrick G. M.: *SADABS, Program for Empirical Absorption Correction of Area Detectors* (Version 2.10). University of Göttingen, Göttingen 2004.
23. Altomare A., Burla M. C., Camalli M., Cascarazo G. L., Giacovazzo C., Guagliardi A., Moliterni A. G. G., Polidori G., Spagna R.: *J. Appl. Crystallogr.* **1999**, *32*, 115.
24. Sheldrick G. M.: *SHELXL97, A Computer Program for the Refinement of Crystal Structures*. University of Göttingen, Göttingen 1997.
25. Farrugia L. J.: *WinGX* (Version 1.64.03b); Farrugia L. J.: *J. Appl. Crystallogr.* **1999**, *32*, 837.
26. Farrugia L. J.: *ORTEP-3 for Windows* (Version 1.076), based on *ORTEP-III* (Version 1.03) by Johnson C. K., Burnett M. N.; Farrugia L. J.: *J. Appl. Crystallogr.* **1997**, *30*, 565.